Geophysical Prospecting, 2006, **54**, 399–407

Vector attenuation: elliptical polarization, raypaths and the Rayleigh-window effect

José M. Carcione*

Istituto Nazionale di Oceanografia e di Geofisica Sperimentale (OGS), Borgo Grotta Gigante 42C, I-34010 Sgonico, Trieste, Italy

Received October 2001, revision accepted December 2005

ABSTRACT

Waves in dissipative media exhibit elliptical polarization. The direction of the major axis of the ellipse deviates from the propagation direction. In addition, Snell's law does not give the raypath, since the propagation (wavevector) direction does not coincide with the energy-flux direction. Each of these physical characteristics depends on the properties of the medium and on the inhomogeneity angle of the wave. The calculations are relevant for multicomponent surveys, where the receivers are placed on the ocean-floor. An example of the role played by inhomogeneous waves is given by the Rayleigh-window effect, which implies a significant amplitude reduction of the reflection coefficient of the ocean-bottom.

INTRODUCTION

Inhomogeneous plane waves in viscoelastic media exhibit elliptical polarization. The degree of ellipticity depends on the inhomogeneity angle (the angle between propagation and attenuation vectors) and the level of attenuation (Buchen 1971; Borcherdt, Glassmoyer and Wennerberg 1986). There are two types of S-wave (Krebes 1983a; Borcherdt and Wennerberg 1985; Borcherdt *et al.* 1986): type-I and type-II S-waves, which are denoted by the symbols SV and SH in seismology (Buchen 1971), although this terminology can be misleading, due to the elliptical character of one of these waves (Borcherdt and Wennerberg 1985). SH-waves have a linear particle motion, perpendicular to the plane made by the propagation and attenuation vectors. The particle motion of the type-I S-wave is elliptical as well as the P-wave particle motion (this can be appreciated in Figs 1, 2, 3 and 7, which show diagrams illustrating the physics).

Winterstein (1987) analysed the variation of the inhomogeneity angle in an anelastic layered medium, and showed that departures from elastic-wave raypaths can be large. In offshore seismic exploration, the waves transmitted at the ocean-bottom have a particular characteristic. According to Snell's law, their attenuation vectors are perpendicular to the ocean-bottom interface, since water is practically lossless. Only at normal incidence are the transmitted waves homogeneous. The inhomogeneity angle can reach values close to 90° (Carcione 1999). Moreover, attenuation can be high, i.e. the energy loss increases with increasing inhomogeneity angle (Borcherdt *et al.* 1986). Quality factor (Q) measurements for marine sediments have been given by Hamilton (1972), with compressional-wave values as low as 5. S-wave Q-factors are not reported, but for unconsolidated materials they should be lower than P-wave Q-factors.

The question then arises of the degree of ellipticity of the particle motion and the deviation of the major axis of the ellipse with respect to the propagation direction. The ellipticity and the deviation are evaluated here for typical marine sediments and under-consolidated reservoir rocks (transition between rocks and sediments). Another feature of wave propagation in dissipative media is the fact that the energy flux (ray) direction does not coincide with the propagation (phase-velocity) direction. As in anisotropic media, the projection of the energy-velocity vector on to the propagation direction is equal to the magnitude of the phase velocity. With anisotropic media, however, this relationship depends not only on the properties of the medium but also on the degree of inhomogeneity of the wave. The latter is a characteristic that depends on the transmission angle at discontinuities (Borcherdt *et al.* 1986; Winterstein 1987). The degree of inhomogeneity is

*E-mail: jcarcione@ogs.trieste.it

significant for large Q contrasts. When investigating the reflection and transmission of SH-waves, Krebes (1983b) found that the transmitted wave is homogeneous when there is no Q contrast, regardless of the value of Q.

The Rayleigh window is an example of the significant role played by inhomogeneous viscoelastic waves. This is a viscoelastic effect, implying that the energy reflected at the boundary, at angles of incidence within that window, is substantially attenuated. Borcherdt *et al.* (1986) presented theoretical and experimental results for a water/stainless-steel interface (e.g. Carcione 2001, p. 214). The phenomenon is associated with elliptical particle motions and strong inhomogeneity angles of the transmitted waves. For P-waves, for instance, the major axis of the ellipse, the propagation direction (wavenumber direction) and the energy-flux direction do not coincide. The amplitude of minimum reflection depends on the shear-wave loss, while the position of the window depends mainly on the shear-wave velocity. These two effects are largely independent. Moreover, the effect is important for hard ocean-bottoms, when the crustal shear-wave velocity is greater than that of the incident P-wave. Fortunately, the window occurs beyond the critical angles, so it is not a problem for pre-critical AVO analyses.

The anelastic model may be relevant for ocean-bottom multicomponent surveys, since the presence of high ellipticities and deviations can make it difficult to identify the P- and S-wave events for polarization/wavefield separation or vector fidelity analysis. In addition, the presence of loss affects the reflection and transmission coefficients of the ocean-bottom and underlying interfaces. Therefore, the present analysis shows how to quantify these effects in order to obtain a better interpretation of multicomponent seismic data.

VECTOR PLANE WAVES, POLARIZATION AND RAYPATHS

The stress-strain relationship for an isotropic viscoelastic medium is given by

$$\sigma_{ij} = \mathcal{E}(t) * \partial_t \epsilon_{kk}\delta_{ij} + 2\mu(t) * (\partial_t \epsilon_{ij} - \partial_t \epsilon_{kk}\delta_{ij}) \tag{1}$$

(Christensen 1982), where σ_{ij} and ϵ_{ij} are the components of the stress and strain tensors, $\mathcal{E}$ and μ are independent relaxation functions, and $*$ denotes time convolution. The relaxation functions correspond to the P-wave modulus $\mathcal{E} = \lambda + 2\mu$ and the rigidity modulus μ, where λ and μ are the Lamé parameters. For notational convenience, we use the same notation in the time and frequency domains.

In general, plane waves in anelastic media have a component of attenuation along the lines of constant phase, which means that their properties are described by two vectors, the attenuation and propagation vectors, which do not point in the same direction. In this section, we summarize the results obtained by Buchen (1971) regarding particle motion associated with these vector plane waves (see also Borcherdt and Wennerberg 1985; Carcione 2001, p. 86).

Let t, $\mathbf{x}$ and ω denote time variable, position vector and angular frequency, respectively, and let $\mathrm{i} = \sqrt{-1}$. We consider the viscoelastic plane-wave solution for the complex potential,

$$\Phi = \Phi_0 \exp[\mathrm{i}(\omega t - \mathbf{k}\cdot\mathbf{x})], \tag{2}$$

where

$$\mathbf{k} = \boldsymbol{\kappa} - \mathrm{i}\boldsymbol{\alpha} = \kappa\hat{\boldsymbol{\kappa}} - \mathrm{i}\alpha\hat{\boldsymbol{\alpha}}, \tag{3}$$

with $\boldsymbol{\kappa}$ and $\boldsymbol{\alpha}$ being the real wavenumber and attenuation vectors, and $\hat{\boldsymbol{\kappa}}$ and $\hat{\boldsymbol{\alpha}}$ being the respective unit vectors. They express the magnitudes of both the wavenumber κ and the attenuation factor α, and the directions of the normals to planes of constant phase and planes of constant amplitude, respectively.

Figure 1 represents the plane wave (2), with γ indicating the inhomogeneity angle. If this angle is zero, the wave is called homogeneous. We note that when $\hat{\boldsymbol{\kappa}}$ is parallel to $\hat{\boldsymbol{\alpha}}$, we have

$$\mathbf{k} = (\kappa - \mathrm{i}\alpha)\hat{\boldsymbol{\kappa}} \equiv k\hat{\boldsymbol{\kappa}}, \tag{4}$$

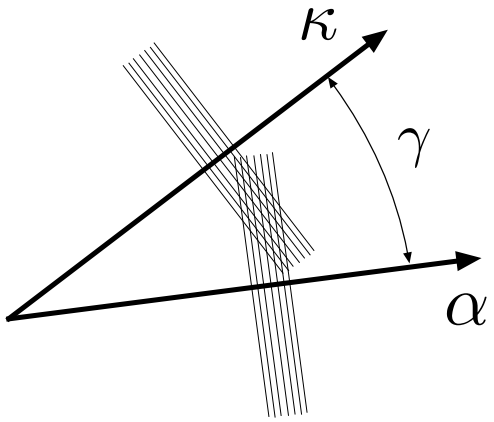

Figure 1 Inhomogeneous viscoelastic plane wave, where the wavenumber vector $\boldsymbol{\kappa}$, the attenuation vector $\boldsymbol{\alpha}$ and the inhomogeneity angle γ are indicated. The planes of constant phase (along $\boldsymbol{\kappa}$) and constant amplitude (along $\boldsymbol{\alpha}$) are also shown. The inhomogeneity angle is less than 90° for this type of wave.

hence $\gamma = 0$ for homogeneous waves. In this case, the complex wavenumber is

$$k = \frac{\omega}{v_c}, \tag{5}$$

where v_c is the complex velocity.

Since the dispersion relationship for inhomogeneous waves can be written as $\mathbf{k} \cdot \mathbf{k} = k^2$ (Buchen 1971), and $\boldsymbol{\kappa} \cdot \boldsymbol{\alpha} = \kappa\alpha \cos\gamma$, solving for κ and α yields

$$2\kappa^2 = \mathrm{Re}(k^2) + \sqrt{[\mathrm{Re}(k^2)]^2 + [\mathrm{Im}(k^2)]^2 \sec^2\gamma},$$
$$2\alpha^2 = -\mathrm{Re}(k^2) + \sqrt{[\mathrm{Re}(k^2)]^2 + [\mathrm{Im}(k^2)]^2 \sec^2\gamma}. \tag{6}$$

We first note that if $\mathrm{Im}(k^2) = 0$, then $\alpha = 0$ and $\gamma = \pi/2$. This case corresponds to an inhomogeneous elastic wave propagating in a lossless material, generated by refraction (a head wave), for instance. In a lossy material, γ must satisfy the condition,

$$0 \le \gamma < \pi/2, \tag{7}$$

because $\alpha \neq 0$ and $\cos\gamma = \hat{\boldsymbol{\kappa}} \cdot \hat{\boldsymbol{\alpha}} \neq 0$.

In the following, we investigate the nature of the P- and S-wave elliptical polarizations, and obtain expressions for the angles between the propagation direction and the major axis of the ellipses.

Particle motion of the P-wave

The P-wave displacement vector can be expressed in terms of the scalar potential Φ as

$$\mathbf{u} = \mathrm{grad}\ \Phi = \mathrm{Re}\{-\mathrm{i}\Phi_0 \mathbf{k} \exp[\mathrm{i}(\omega t - \mathbf{k} \cdot \mathbf{x})]\}. \tag{8}$$

Using (3) and $\Phi_0 k = |\Phi_0 k| \exp[\mathrm{i}\arg(\Phi_0 k)]$, we obtain

$$\mathbf{u} = -|\Phi_0 k| \exp(-\boldsymbol{\alpha} \cdot \mathbf{x})\ \mathrm{Re}\left[\mathrm{i}\left(\frac{v_c}{\omega}\right)\mathbf{k} \exp(\mathrm{i}\varsigma)\right], \tag{9}$$

where

$$\varsigma(t) = \omega t - \boldsymbol{\kappa} \cdot \mathbf{x} + \arg(\Phi_0 k), \tag{10}$$

and (5) has been used (v_c represents the P-wave complex velocity.) We introduce the real vectors $\boldsymbol{\xi}_1$ and $\boldsymbol{\xi}_2$, such that

$$\left(\frac{v_c}{\omega}\right)\mathbf{k} = \left(\frac{v_c}{\omega}\right)(\boldsymbol{\kappa} - \mathrm{i}\boldsymbol{\alpha}) = \boldsymbol{\xi}_1 + \mathrm{i}\boldsymbol{\xi}_2, \tag{11}$$

where

$$\omega\boldsymbol{\xi}_1 = v_R\boldsymbol{\kappa} + v_I\boldsymbol{\alpha}, \quad \omega\boldsymbol{\xi}_2 = v_I\boldsymbol{\kappa} - v_R\boldsymbol{\alpha}, \tag{12}$$

and v_R and v_I denote the real and imaginary parts of v_c; they depend only on the intrinsic quality factor of the medium and not on the degree of inhomogeneity of the wave.

These vectors are orthogonal, thus

$$\boldsymbol{\xi}_1 \cdot \boldsymbol{\xi}_2 = 0, \tag{13}$$

and they satisfy the condition,

$$\xi_1^2 - \xi_2^2 = 1. \tag{14}$$

Substituting (11) into (9) gives

$$\mathbf{u} = U_0(\boldsymbol{\xi}_1 \sin\varsigma + \boldsymbol{\xi}_2 \cos\varsigma), \tag{15}$$

and eliminating ς yields

$$\frac{U_1^2}{\xi_1^2} + \frac{U_2^2}{\xi_2^2} = 1, \tag{16}$$

where

$$U_1 = \frac{\mathbf{u} \cdot \boldsymbol{\xi}_1}{\xi_1 U_0}, \quad U_2 = -\frac{\mathbf{u} \cdot \boldsymbol{\xi}_2}{\xi_2 U_0}, \tag{17}$$

with

$$U_0 = |\Phi_0 k| \exp(-\boldsymbol{\alpha} \cdot \mathbf{x}). \tag{18}$$

Equation (16) indicates that the particle motion is an ellipse, with major axis $\boldsymbol{\xi}_1$ and minor axis $\boldsymbol{\xi}_2$ (see Fig. 2). The direction of rotation is from $\boldsymbol{\kappa}$ to $\boldsymbol{\alpha}$, with the angle between the

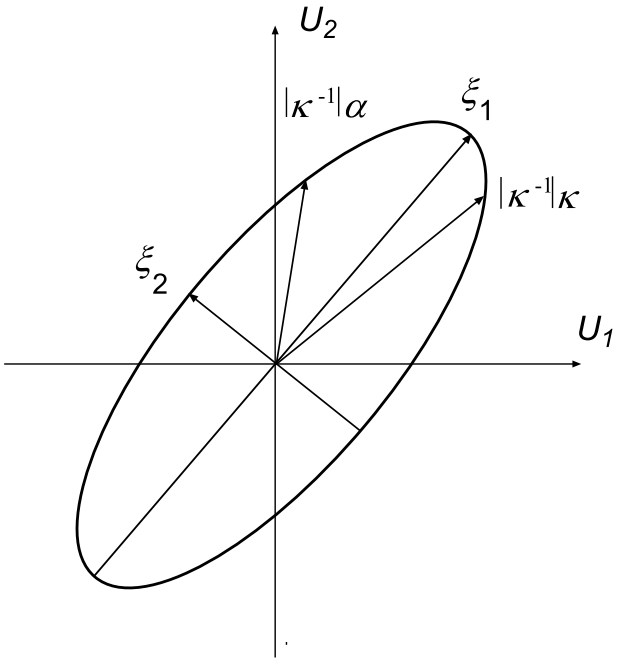

Figure 2 Particle motion of an inhomogeneous P-wave in an isotropic viscoelastic medium (Buchen 1971). The propagation and attenuation directions and their relationships with vectors $\boldsymbol{\xi}_1$ and $\boldsymbol{\xi}_2$ are also shown. The ellipse degenerates into a straight line for a homogeneous plane wave.

propagation direction and the major axis of the ellipse given by

$$\cos\psi = \frac{\boldsymbol{\kappa}\cdot\boldsymbol{\xi}_1}{\kappa\xi_1} = \frac{1}{\omega\xi_1}(v_{\rm R}\kappa + v_{\rm I}\alpha\cos\gamma), \tag{19}$$

where we have used (12).

For a homogeneous plane wave, the ellipse degenerates into a straight line.

Particle motion of the type-I S-wave

The particle motion of the type-I S-wave shows similar characteristics to the P-wave particle motion. Its displacement vector can be expressed in terms of a vector potential,

$$\boldsymbol{\Theta} = \Theta_0\hat{\mathbf{n}}\exp[{\rm i}(\omega t - \mathbf{k}\cdot\mathbf{x})], \tag{20}$$

as

$$\mathbf{u} = \text{curl}\ \boldsymbol{\Theta} = {\rm Re}\{-{\rm i}\Theta_0(\hat{\mathbf{n}}\times\mathbf{k})\exp[{\rm i}(\omega t - \mathbf{k}\cdot\mathbf{x})]\}, \tag{21}$$

which lies in the plane of $\boldsymbol{\kappa}$ and $\boldsymbol{\alpha}$. The unit vector $\hat{\mathbf{n}}$ is perpendicular to the $(\boldsymbol{\kappa}, \boldsymbol{\alpha})$-plane. To avoid ambiguities in the case of homogeneous waves, we may assume that $\hat{\mathbf{n}}$ is defined as perpendicular to the sagittal plane. For instance, in the case of surface waves travelling in the half-space $z \geq 0$, this plane is defined by the direction of propagation (say, the x-direction) and the orthogonal direction z.

For simplicity, we use the same notation as for the P-wave but, here, the complex velocity $v_{\rm c}$ is equal to the shear-wave complex velocity. Using (3) and $\Theta_0 k = |\Theta_0 k|\exp[{\rm i}\arg(\Theta_0 k)]$, we obtain

$$\mathbf{u} = -|\Theta_0 k|\exp(-\boldsymbol{\alpha}\cdot\mathbf{x}){\rm Re}\left[{\rm i}\left(\frac{v_{\rm c}}{\omega}\right)(\hat{\mathbf{n}}\times\mathbf{k})\exp({\rm i}\varsigma)\right], \tag{22}$$

where

$$\varsigma(t) = \omega t - \boldsymbol{\kappa}\cdot\mathbf{x} + \arg(\Theta_0 k). \tag{23}$$

As before, $v_{\rm c}\mathbf{k}/\omega$ can be decomposed into real and imaginary vectors as in (11). Let us define

$$\left(\frac{v_{\rm c}}{\omega}\right)\hat{\mathbf{n}}\times\mathbf{k} = \boldsymbol{\zeta}_1 + {\rm i}\boldsymbol{\zeta}_2, \tag{24}$$

Substituting (24) into (22) gives

$$\mathbf{u} = U_0(\boldsymbol{\zeta}_1\sin\varsigma + \boldsymbol{\zeta}_2\cos\varsigma), \tag{25}$$

where

$$U_0 = |\Theta_0 k|\exp(-\boldsymbol{\alpha}\cdot\mathbf{x}) \tag{26}$$

and

$$\boldsymbol{\zeta}_1 = \hat{\mathbf{n}}\times\boldsymbol{\xi}_1, \quad \boldsymbol{\zeta}_2 = \hat{\mathbf{n}}\times\boldsymbol{\xi}_2, \tag{27}$$

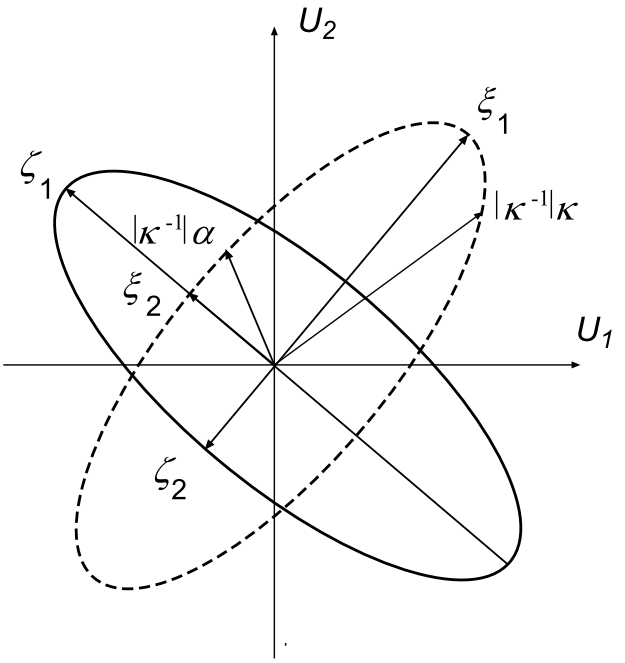

Figure 3 Particle motion of an inhomogeneous type-I S-wave in an isotropic viscoelastic medium (Buchen 1971). The propagation and attenuation directions and their relationships with vectors $\boldsymbol{\xi}_1$, $\boldsymbol{\xi}_2$, $\boldsymbol{\zeta}_1$ and $\boldsymbol{\zeta}_2$ are also shown. The ellipse degenerates into a straight line for a homogeneous plane wave.

with $\boldsymbol{\xi}_1$ and $\boldsymbol{\xi}_2$ given by (12), but using the S-wave complex velocity instead of the P-wave complex velocity. These vectors have the properties

$$\boldsymbol{\zeta}_1\cdot\boldsymbol{\zeta}_2 = 0, \quad \zeta_1^2 - \zeta_2^2 = 1. \tag{28}$$

The particle motion is an ellipse, whose major and minor axes are given by $\boldsymbol{\zeta}_1$ and $\boldsymbol{\zeta}_2$, respectively. The direction of rotation is from $\boldsymbol{\kappa}$ to $\boldsymbol{\alpha}$, with the angle between the propagation direction and the major axis of the ellipse given by

$$\cos\psi = \frac{\boldsymbol{\kappa}\cdot\boldsymbol{\zeta}_1}{\kappa\zeta_1} = \frac{v_{\rm I}\alpha\sin\gamma}{\omega\zeta_1}. \tag{29}$$

Figure 3 shows a diagram of the S-wave particle motion. For a homogeneous plane wave, the ellipse degenerates into a straight line.

Raypaths

In this section, we obtain the angle between the propagation and ray directions, where the raypath is defined by the energy-velocity direction. The phase- and energy-velocity vectors do not point in the same direction in isotropic viscoelastic media (Buchen 1971; Carcione 2001, p. 99). Phase- and

energy-velocity vectors are equal only for homogeneous waves ($\gamma = 0$). We do not consider the group velocity concept, since it loses physical meaning in viscoelastic media (Ben-Menahem and Singh 1981; Carcione 2001, p. 146).

Let $\mathbf{v}_p$ and $\mathbf{v}_e$ be the phase- and energy-velocity vectors. For inhomogeneous waves, we have

$$\hat{\boldsymbol{\kappa}} \cdot \mathbf{v}_e = v_p \tag{30}$$

(Buchen 1971; Carcione 2001, p. 99), where $\hat{\boldsymbol{\kappa}}$ is a unit vector along the phase-velocity (propagation) direction, and

$$v_p = \frac{\omega}{\kappa} \tag{31}$$

is the magnitude of the phase velocity.

The energy-velocity vector is defined as the ratio of the time-averaged Umov-Poynting vector (energy-flux vector) to the time average of the total energy density. It is given by

$$\mathbf{v}_e = \frac{\omega\Big[\rho\omega^2\boldsymbol{\kappa} + 4(\boldsymbol{\kappa}\times\boldsymbol{\alpha})\times(\mu_I\boldsymbol{\kappa} - \mu_R\boldsymbol{\alpha})\Big]}{\rho\omega^2\kappa^2 + 4\mu_R|\boldsymbol{\kappa}\times\boldsymbol{\alpha}|^2} \tag{32}$$

(Buchen 1971; Carcione 2001, p. 98–99), where ρ is the density and μ_R and μ_I are the real and imaginary parts of the complex shear modulus μ.

Then, using the preceding equations, the cosine of the angle between the propagation and ray directions is given by

$$\cos\phi = \frac{v_p}{v_e} = \frac{\kappa\Big(\rho\omega^2 + 4\mu_R|\hat{\boldsymbol{\kappa}}\times\boldsymbol{\alpha}|^2\Big)}{\Big|\rho\omega^2\boldsymbol{\kappa} + 4(\boldsymbol{\kappa}\times\boldsymbol{\alpha})\times(\mu_I\boldsymbol{\kappa} - \mu_R\boldsymbol{\alpha})\Big|}. \tag{33}$$

Using the expansion $(\mathbf{a}\times\mathbf{b})\times\mathbf{c} = \mathbf{b}(\mathbf{c}\cdot\mathbf{a}) - \mathbf{a}(\mathbf{b}\cdot\mathbf{c})$, (33) becomes

$$\cos\phi = \frac{\kappa\Big(\rho\omega^2 + 4\mu_R\alpha^2\sin^2\gamma\Big)}{\sqrt{A^2\kappa^2 + B^2\alpha^2 + 2AB\kappa\alpha\cos\gamma}}, \tag{34}$$

where

$$A = \rho\omega^2 - 4\mu_I\kappa\alpha\cos\gamma + 4\mu_R\alpha^2 \quad \text{and}$$
$$B = 4(\mu_I\kappa^2 - \mu_R\kappa\alpha\cos\gamma). \tag{35}$$

The energy- and phase-velocity directions do not coincide with the directions defined by the axes of the polarization ellipse. Note that in the homogeneous lossless case, the energy-velocity vector is equal to the phase-velocity vector and the particle motion is linear, with the polarization parallel (P-waves) and perpendicular (S-waves) to those vectors.

CONSTANT-Q MODEL

We consider a constant-Q model to describe attenuation. Kjartansson's model of constant Q (Caputo and Mainardi 1971; Kjartansson 1979; Carcione 2001, p. 73), extended to isotropic viscoelastic media, implies the following P- and S-wave complex velocities:

$$v_P = \sqrt{\frac{\mathcal{E}(\omega)}{\rho}} \quad \text{and} \quad v_S = \sqrt{\frac{\mu(\omega)}{\rho}}. \tag{36}$$

The dynamic moduli $\mathcal{E}$ and μ are given by

$$\mathcal{E}(\omega) = \mathcal{E}_0\left(\frac{\mathrm{i}\omega}{\omega_0}\right)^{2\eta_\mathcal{E}} \quad \text{and} \quad \mu(\omega) = \mu_0\left(\frac{\mathrm{i}\omega}{\omega_0}\right)^{2\eta_\mu}, \tag{37}$$

where

$$\eta_\mathcal{E} = \frac{1}{\pi}\tan^{-1}\left(\frac{1}{Q_P}\right), \qquad \eta_\mu = \frac{1}{\pi}\tan^{-1}\left(\frac{1}{Q_S}\right), \tag{38}$$

Q_P and Q_S are the P-wave and S-wave quality factors, respectively, and ω_0 is a reference frequency. We see that $Q > 0$ is equivalent to $0 < \eta < 1/2$. The moduli $\mathcal{E}_0$ and μ_0 can be expressed in terms of the P-wave and S-wave velocities, c_P and c_S, as

$$\mathcal{E}_0 = \rho c_P^2\cos^2\left(\frac{\pi\eta_\mathcal{E}}{2}\right) \quad \text{and} \quad \mu_0 = \rho c_S^2\cos^2\left(\frac{\pi\eta_\mu}{2}\right), \tag{39}$$

where c_P and c_S are the P-wave and S-wave phase velocities at the reference frequency ω_0 (Carcione 2001, p. 74).

The quality factor for homogeneous plane waves ($\gamma = 0$) is given by

$$Q = -\frac{\mathrm{Re}(k^2)}{\mathrm{Im}(k^2)} = \frac{\mathrm{Re}\left(v_c^2\right)}{\mathrm{Im}\left(v_c^2\right)} \tag{40}$$

(Carcione 2001, p. 87), where Q is Q_P or Q_S, depending on the wave type. Equation (40), together with (5) and (36), implies

$$Q_P = \frac{\mathrm{Re}(\mathcal{E})}{\mathrm{Im}(\mathcal{E})} \quad \text{and} \quad Q_S = \frac{\mathrm{Re}(\mu)}{\mathrm{Im}(\mu)}, \tag{41}$$

which do not depend on frequency and correspond to the quality factors of homogeneous waves.

EXAMPLES

Let us consider the case, $c_P = 1900$ m/s, $c_S = 900$ m/s, $\rho = 1300$ kg/m^3, $Q_S = 0.6Q_P$, and the following values of Q_P: 5, 10, 15, 20 and 30. Assume a reference frequency $\omega_0 = 2\pi \times 30$ Hz and a frequency $\omega = \omega_0$. At this frequency, the P-wave and S-wave phase velocities are equal to c_P and c_S, respectively. We define the ellipticity as $(\xi_1 - \xi_2)/\xi_1$ for P-waves, and $(\zeta_1 - \zeta_2)/\zeta_1$ for type-I S-waves. Homogeneous waves ($\gamma = 0$) have an ellipticity equal to 1, indicating linear polarization. Figure 4(a,b) shows the ellipticity and deviation of the major axis (with respect to the propagation direction) of the P-wave

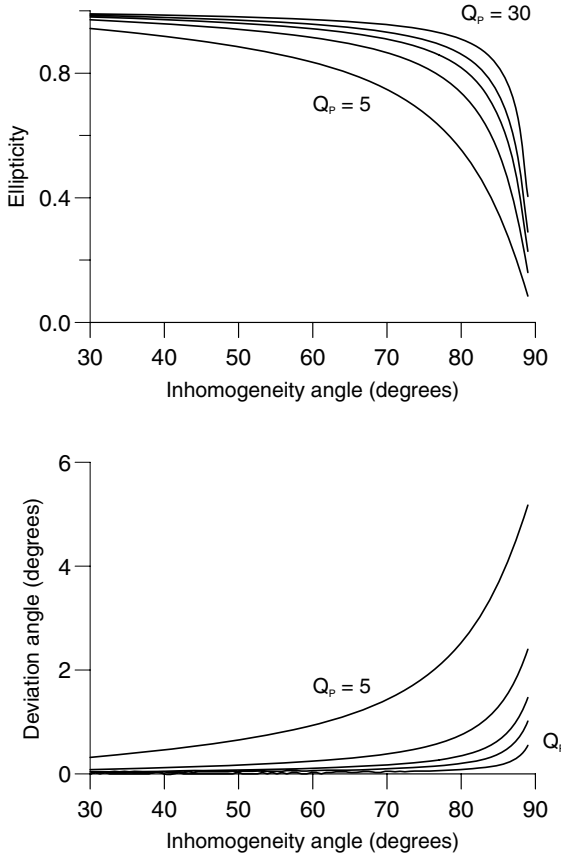

Figure 4 Ellipticity and deviation of the major axis of the P-wave (with respect to the propagation direction) versus the inhomogeneity angle γ. The ellipse becomes a circle when the inhomogeneity angle approaches 90°, and the ellipticity is defined such that it is equal to 1 for linear particle motions and 0 for circular particle motions.

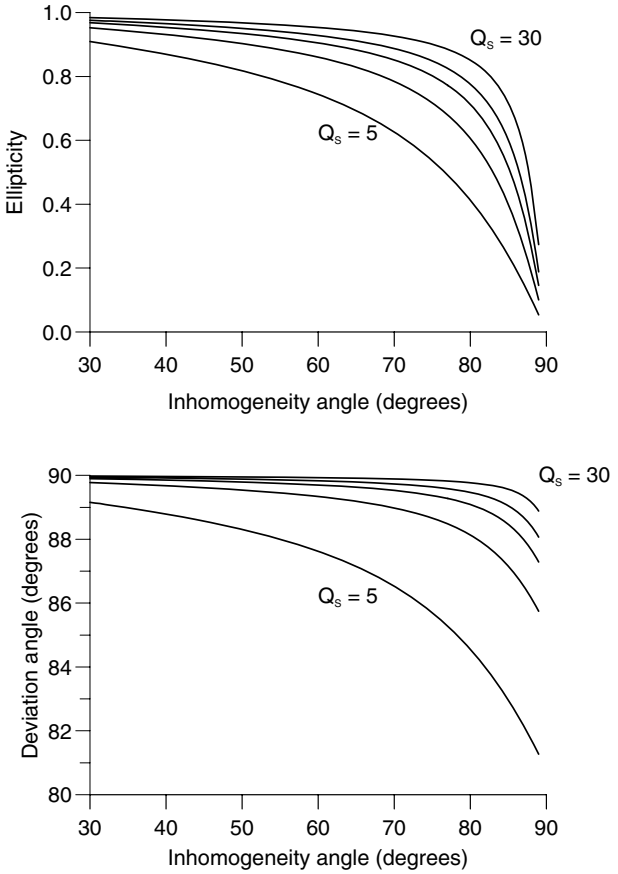

Figure 5 Ellipticity and deviation of the major axis of the type-I S-wave (with respect to the propagation direction) versus the inhomogeneity angle γ. The ellipse becomes a circle when the inhomogeneity angle approaches 90°.

versus the inhomogeneity angle γ. Figure 5(a,b) shows the curves corresponding to the S-wave. The value of Q_P is indicated in the figures. The ellipse becomes a circle when the inhomogeneity angle approaches 90°. Deviations from linear polarization are important for low Q-values, particularly for the S-waves. Figure 6 shows the angle between the propagation (phase) direction and ray (energy) direction versus the inhomogeneity angle γ and various values of the P-wave quality factor, for a P-wave (a) and a type-I S-wave (b).

Numerical simulation of the Rayleigh-window effect

One of the most striking features of the anelastic model is the prediction of the phenomenon termed the anelastic Rayleigh window. Brekhovskikh (1960, p. 34) observed that the amplitude reflection coefficient measured for a water/steel interface was not consistent with that predicted by the elastic theory. Beyond the elastic S-wave critical angle, there is a reduction in amplitude of the reflected P-wave in a narrow window. Because this occurs for an angle where the apparent phase velocity of the incident wave is near that of the Rayleigh surface wave, the phenomenon is called the 'Rayleigh window' (Carcione 2001, p. 214). The corresponding reflection coefficient was measured experimentally by Becker and Richardson (1972), and their ultrasonic experiments were verified with an anelastic model.

The problem was investigated by Borcherdt *et al.* (1986), who found that the Rayleigh window should be observable in appropriate sets of wide-angle reflection data and that this can be useful in estimating attenuation for various ocean-bottom reflectors. Figure 7 shows a homogeneous acoustic wave, incident on the ocean-bottom interface, and the corresponding reflected and transmitted waves. The wavenumber and attenuation vectors are indicated. Except at normal incidence, the transmitted waves are inhomogeneous with elliptical particle motion and the inhomogeneity angle is equal to the

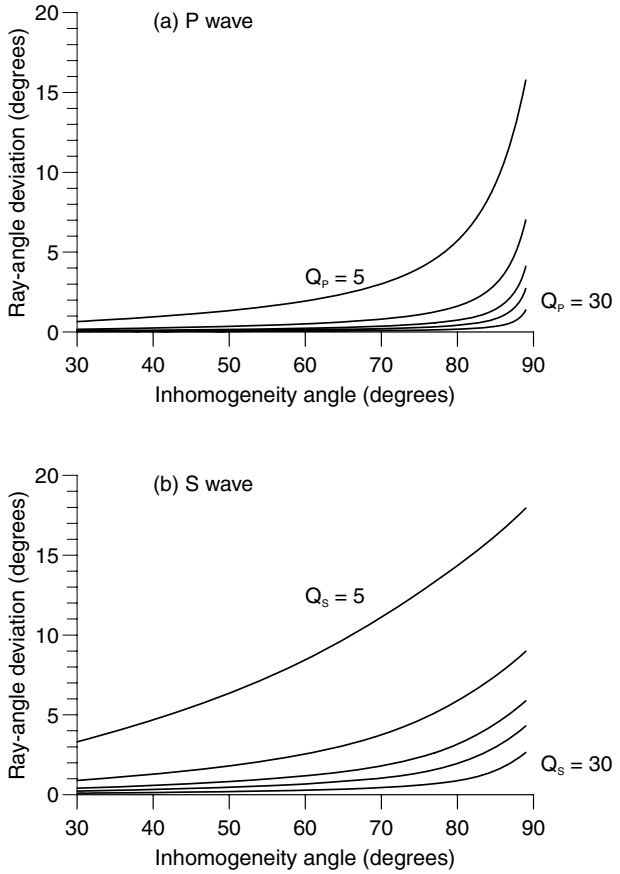

Figure 6 Angle between the propagation direction and ray direction versus the inhomogeneity angle γ: (a) for a P-wave; (b) for a type-I S-wave.

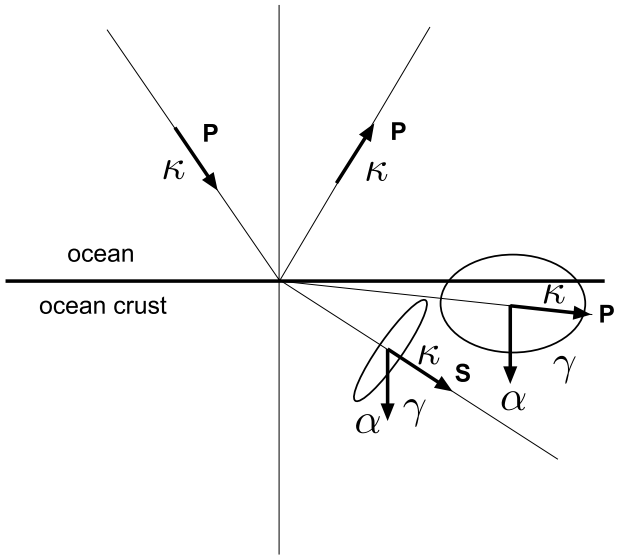

Figure 7 Homogeneous acoustic wave incident on the ocean-bottom interface, and reflected and transmitted waves. The wavenumber and attenuation vectors are indicated. Except at normal incidence, the transmitted waves are inhomogeneous with elliptical particle motion.

transmission angle. In fact, because of the very weak attenuation of water, the attenuation vectors have negligible magnitude in the ocean, and are approximately perpendicular to the interface in the ocean crust (viscoelastic Snell's law; see e.g. Carcione 2001, p. 100).

The presence of inhomogeneous viscoelastic waves accounts for the existence of the anelastic Rayleigh window. Let us consider an example, where the properties of water are $c_P = 1490$ m/s, $\rho = 1000$ kg/m^3 and $Q_P = 10\,000$ at 20 Hz. The unrelaxed velocities of the ocean-bottom are $c_P = 4850$ m/s and $c_S = 2800$ m/s, the density is $\rho = 2600$ kg/m^3, and the quality factors at 20 Hz are $Q_P = 1000$ and $Q_S = 10$. In this case, anelasticity is described by the Zener model (Ben-Menahem and Singh 1981). The analytical expression for the reflection and transmission coefficients can be found in Becker and Richardson (1972) and Carcione (2001, p. 213). When the angle of incidence approaches the elastic S-wave critical angle, the inhomogeneity angle of the the transmitted S-wave increases asymptotically to a value near but not equal to 90°, and the ellipticity decreases substantially. This is shown in Fig. 8, where the inhomogeneity angle and ellipticity of the transmitted S-wave are plotted versus the angle of incidence. As can be seen, at the location of the window (an angle of incidence of nearly 37°), there is a transition where the wave becomes highly inhomogeneous. Similarly, for angles of incidence in the window, the transmitted P-wave has an inhomogeneity angle near to but less than 90° and the particle motion becomes elliptical with very low ellipticity values (Borcherdt *et al.* 1986).

We perform a numerical evaluation of the reflection coefficient versus incidence angle from synthetic data generated by a viscoelastic modelling algorithm. We generate synthetic seismograms with a time-domain modelling algorithm, based on the viscoelastic wave equation and a domain decomposition technique, where two grids model the fluid and the solid subdomains (Carcione 1996). Anelasticity is described in terms of memory variables (Carcione 2001, p. 110). The solution on each grid is obtained by using the Runge–Kutta method as a time-stepping algorithm and the Fourier and Chebyshev differential operators to compute the spatial derivatives in the horizontal and vertical directions, respectively (Carcione 1996; Carcione 2001, p. 320). The technique to obtain the reflection coefficients from synthetic seismograms has been used by Kindelan, Seriani and Sguazzero (1989) for lossless media.

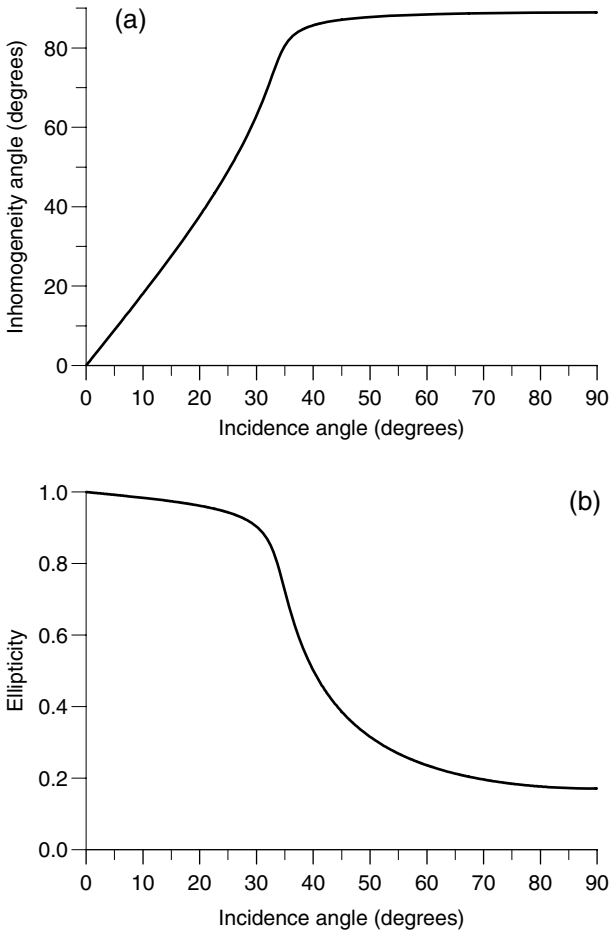

Figure 8 Inhomogeneity angle (a) and ellipticity (b) of the transmitted S-wave at the ocean-bottom interface versus the angle of incidence.

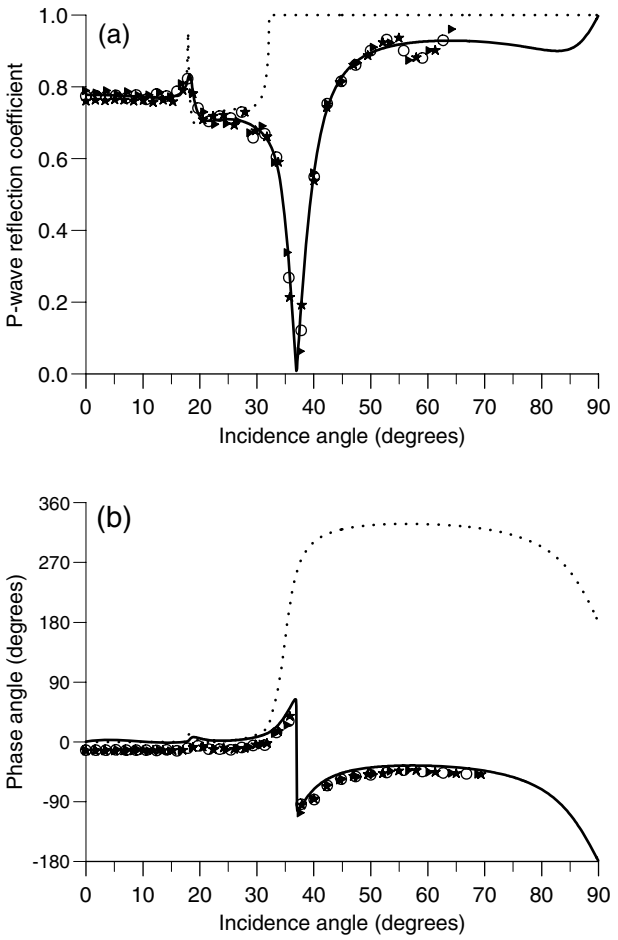

Figure 9 The Rayleigh window at the ocean-bottom interface. P-wave reflection coefficient (a) and phase angle (b) versus angle of incidence. The symbols, i.e. circles, triangles and asterisks, correspond to a numerical evaluation of the reflection coefficient at 19, 20 and 21 Hz, respectively. The dotted line corresponds to the prediction of the elastic theory.

Figure 9 shows the numerical evaluation of the P-wave reflection coefficient (a) and phase angle (b), where the dotted line corresponds to the prediction of the elastic theory. The mismatch between theory and numerical experiments is due to the fact that the receivers are located 1.3 m above the interface. There is then a phase shift of nearly 12° between the incident wave and the reflected wave. As can be seen, the elastic theory fails to predict the correct physical behaviour for angles greater than 30°.

It is difficult to observe the Rayleigh-window phenomenon in the space–time domain, since the reflected pulse is masked by the head wave, because the window is located beyond the critical angle. The results in Fig. 9 constitute a confirmation of the correctness of the anelastic model, and the significant role that inhomogeneity plays in wave propagation.

CONCLUSIONS

As shown by Winterstein (1987), small changes in the inhomogeneity angle γ of the incident wave around the angle of incidence can translate to very large changes in γ of waves in deeper layers. Reflected and transmitted P- and S-waves may have magnitudes of γ near 90° when reaching the ocean-floor (or the surface in on-shore exploration). This fact and the presence of strong attenuation in the upper layers imply significant deviations from linear polarization. Inhomogeneous waves exhibit an anisotropic-like behaviour of the energy- and phase-velocity vectors, which, in addition, depends on the degree of inhomogeneity. The latter is a property of the wave and not of the medium. The raypath direction does not

coincide with the propagation direction; that is, Snell's law does not give the ray direction, which is given by the energy-velocity vector. Deviations between the propagation and ray directions can reach angles of 20° for unconsolidated sediments and inhomogeneity angles close to 90°. These calculations may be relevant for ocean-bottom multicomponent surveys, where the presence of high ellipticities can make the identification of P- and S-wave events difficult when using methods based on polarization measurements. An illustration of the significant role that inhomogeneity can play in seismology is given by the Rayleigh-window effect, where the transmitted P- and S-waves reach inhomogeneity angles close to 90° and the respective particle motions depart significantly from linearity, implying low ellipticity values.

ACKNOWLEDGEMENTS

This work was financed by Norsk Hydro (Bergen) and the Universidade Federal da Bahia (Salvador). I am grateful to Hans B. Helle and M. A. B. Botelho for useful discussions, and to M. van der Baan and Paul Williamson for detailed reviews.

REFERENCES

Becker F.L. and Richardson R.L. 1972. Influence of material properties on Rayleigh critical-angle reflectivity. *Journal of the Acoustical Society of America* **51**, 1609–1617.

Ben-Menahem A. and Singh S.G. 1981. *Seismic Waves and Sources*. Springer Verlag, Inc.

Borcherdt R.D., Glassmoyer G. and Wennerberg L. 1986. Influence of welded boundaries in anelastic media on energy flow, and characteristics of *P*, *S*-I and *S*-II waves: observational evidence for inhomogeneous body waves in low-loss solids. *Journal of Geophysical Research* **91**, 11 503–11 118.

Borcherdt R.D. and Wennerberg L. 1985. General *P*, type-I *S*, and type-II *S* waves in anelastic solids: Inhomogeneous wave fields in low-loss solids. *Bulletin of the Seismological Society of America* **75**, 1729–1763.

Brekhovskikh L.M. 1960. *Waves in Layered Media*. Academic Press, Inc.

Buchen P.W. 1971. Plane waves in linear viscoelastic media. *Geophysical Journal of the Royal Astronomical Society* **23**, 531–542.

Caputo M. and Mainardi F. 1971. Linear models of dissipation in anelastic solids. *Rivista del Nuovo Cimento* (Ser. II) **1**, 161–198.

Carcione J.M. 1996. Elastodynamics of a non-ideal interface: Application to crack and fracture scattering. *Journal of Geophysical Research* **101**(B12), 28 177–28 188.

Carcione J.M. 1999. The effects of vector attenuation on AVO of off-shore reflections. *Geophysics* **64**, 815–819.

Carcione J.M. 2001. Wave fields in real media: Wave propagation in anisotropic, anelastic and porous media. *Handbook of Geophysical Exploration* **31**. Pergamon Press, Inc.

Christensen R.M. 1982. *Theory of Viscoelasticity*. Academic Press, Inc.

Hamilton E. 1972. Compressional wave attenuation in marine sediments. *Geophysics* **37**, 620–646.

Kindelan M., Seriani G. and Sguazzero P. 1989. Elastic modelling and its application to amplitude versus angle interpretation. *Geophysical Prospecting* **37**, 3–30.

Kjartansson E. 1979. Constant *Q*-wave propagation and attenuation. *Journal of Geophysical Research* **84**, 4737–4748.

Krebes E.S. 1983a. Discrepancies in energy calculations for inhomogeneous waves. *Geophysical Journal of the Royal Astronomical Society* **75**, 839–846.

Krebes E.S. 1983b. The viscoelastic reflection/transmission problem: two special cases. *Bulletin of the Seismological Society of America* **73**, 1673–1683.

Winterstein D.F. 1987. Vector attenuation: Some implications for plane waves in anelastic layered media. *Geophysics* **52**, 810–814.